ChemComm

COMMUNICATION

View Article Online
View Journal | View Issue

Cite this: *Chem. Commun.*, 2025, **61**, 11681

Received 24th February 2025,
Accepted 27th May 2025

DOI: 10.1039/d5cc01008j

rsc.li/chemcomm

Decorated high-dispersity $Fe(OH)_3$ nanoparticles on NiZn LDH nanosheets towards enhanced alkaline oxygen evolution reaction†

Tianyi Yang,[a] Jianfeng Huang,[a] Zhaohui Liu*[a] and Cailing Chen*[b]

The creation of efficient, earth-abundant electrocatalysts is crucial to address the sluggish kinetics of the oxygen evolution reaction (OER). In this study, a straightforward immersion technique is employed to fabricate a $NiZnFe_x$ LDH composite by embedding $Fe(OH)_3$ nanoparticles onto NiZn LDH nanosheets. The optimized $NiZnFe_{12.9}$ LDH catalyst exhibits an overpotential of just 191 mV at 10 mA cm^{-2}, significantly outperforming traditional OER catalysts. Additionally, it demonstrates exceptional long-term stability, maintaining a current density of 120 mA cm^{-2} for more than 125 hours. This approach fosters the advancement of materials for water splitting and hydrogen production, which are crucial for sustainable energy solutions.

Hydrogen is increasingly recognized as a clean alternative to fossil fuels, offering a promising solution for sustainable energy systems. Electrochemical water electrolysis, which produces high-purity hydrogen, plays a key role in this field.[1–3] The OER is a critical yet energy-intensive half-reaction in water electrolysis, involving complex electron transfer steps that create significant energy barriers. As a result, developing highly efficient OER electrocatalysts is essential for improving the efficiency of water splitting and enabling scalable hydrogen production.[4,5] Research into OER electrocatalysts has prioritized materials that reduce overpotentials to lower energy demands. Despite the superior activity of IrO_2 and RuO_2, their scarcity and cost limit large-scale use.[6] Consequently, efforts now focus on developing efficient, durable catalysts from earth-abundant metals to enable sustainable and scalable OER technologies.

Layered double hydroxides (LDHs) offer significant potential in electrocatalysis due to their low cost, abundance, and compositional flexibility.[7,8] However, challenges such as poor conductivity and limited active site exposure hinder their OER efficiency. Strategies like exfoliation,[9,10] etching,[11,12] decoration,[13,14] and doping[15,16] have been employed to enhance active site accessibility, conductivity, and surface area. These advancements not only improve intrinsic properties but also optimize the electrochemical performance, making it a promising electrocatalyst.

Nickel (Ni), cobalt (Co), and zinc (Zn)-based LDHs have emerged as promising catalysts for the OER, owing to their favorable catalytic properties. Incorporating iron (Fe) into these materials, such as in Fe–Ni and Fe–Co LDHs, has been shown to significantly enhance catalytic performance compared to their iron-free counterparts, like $Ni(OH)_2$ and $Co(OH)_2$.[17–19] This enhancement is attributed to Fe's ability to generate additional active sites, improving catalyst efficiency. Furthermore, combining Fe with other materials, such as metal–organic frameworks (MOFs) or metal oxides, can increase active sites and boost electrochemical properties, enhancing OER effectiveness.[20,21] This strategy not only improves activity but also enhances the stability of the catalysts, which is essential for their practical use in renewable energy applications.

Among conventional transition metal (Fe, Co, Ni) hydroxides used in the OER, Fe hydroxide stands out due to two critical merits. First, the crustal abundance of iron surpasses other transition metals, which offers economic advantages for scalable electrocatalyst development. Secondly, Fe hydroxide outperforms Co hydroxide and Ni hydroxide in single-component OER activity ($FeO_xH_y > CoO_xH_y > NiO_xH_y$), as experimentally validated.[22] Recent works have also demonstrated that immobilizing iron hydroxide on other substrates can significantly enhance the OER activity, due to the abundant active surfaces/interfaces generated.[23,24]

Based on the aforementioned considerations, $Fe(OH)_3$-decorated composites have been synthesized by anchoring highly dispersed $Fe(OH)_3$ nanoparticles onto NiZn LDH nanosheets. This approach effectively combines the electrochemical advantages of both Fe and NiZn, resulting in a trimetallic

[a] *State Key Laboratory of Coal Mine Disaster Dynamics and Control, Institute of Advanced Interdisciplinary Studies, School of Chemistry and Chemical Engineering, Chongqing University, Chongqing 400044, China. E-mail: zhaohui.liu@cqu.edu.cn*
[b] *Advanced Membranes and Porous Materials (AMPM) Center, Physical Science and Engineering Division, King Abdullah University of Science and Technology (KAUST), Thuwal, 23955, Saudi Arabia. E-mail: cailing.chen@kaust.edu.sa*

† Electronic supplementary information (ESI) available. See DOI: https://doi.org/10.1039/d5cc01008j

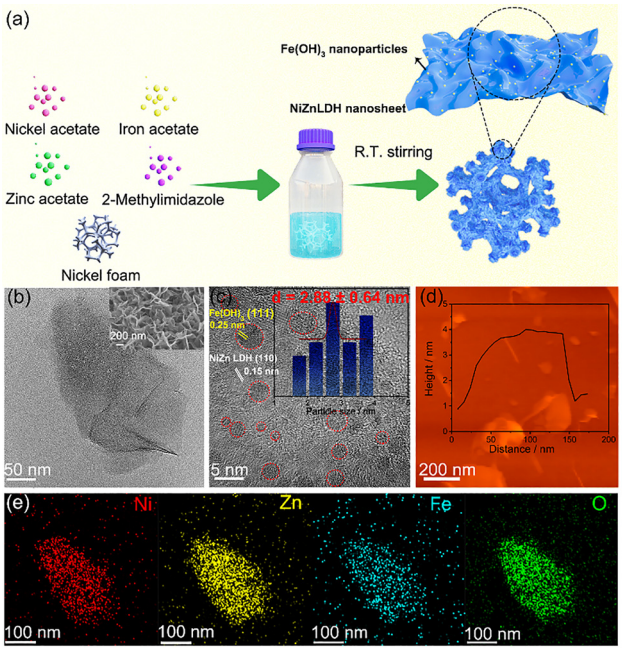

Fig. 1 (a) Synthetic procedure of the $NiZnFe_x$ LDH nanosheets. (b) TEM and SEM (inset) image; (c) HRTEM image and size distribution diagram (inset); (d) AFM image and height profile; (e) EDS mapping of the $NiZnFe_{12.9}$ LDH nanosheets.

hydroxide structure. The resulting 2D trimetallic nanosheets demonstrate both high activity and long-term stability under alkaline OER conditions, which are typically challenging for many catalysts. The synergistic interaction between Fe, Ni, and Zn within the structure not only enhances the accessibility of the active sites but also improves conductivity, thereby facilitating efficient electron transfer during the OER process.

As shown in Fig. 1a, trimetallic NiZnFe LDH nanosheets were successfully synthesized on nickel foam using a simple one-pot solution method at a moderate temperature. Inspired by the imidazole ligand assisted approach conducted at ambient temperature and pressure,[25] this process involved reacting Ni/Zn/Fe precursors with 2-methylimidazole. By regulating the Fe dosage, a series of $NiZnFe_x$ LDH samples (where x = 2.6, 8.9, 12.9, 23.7 represents the Fe content by weight (wt%), as determined by ICP-OES) were obtained. TEM and SEM observations confirmed that NiZn LDH and $NiZnFe_x$ LDH exhibited an ultrathin nanosheet structure with a height of 3–5 nm (Fig. 1b and Fig. S1–S4, ESI†). Interestingly, according to the HRTEM image, highly dispersed small $Fe(OH)_3$ nanoparticles can be observed on the nanosheet substance, with an average size of 2.68 ± 0.64 nm. The increasing Fe content led to larger $Fe(OH)_3$ nanoparticles with an average size of 7.41 ± 1.64 nm ($NiZnFe_{12.9}$ LDH, Fig. S4b, ESI†). The HRTEM image (Fig. 1c) reveals a lattice spacing of 0.15 nm on the NiZnFe LDH nanosheets, which well matched the (110) facet of Ni(Zn)-LDH. Additionally, the lattice spacing of the smaller nanoparticles was measured to be 0.25 nm, aligning with the (111) facet of $Fe(OH)_3$ (Fig. 1c). The thickness of $NiZnFe_{12.9}$ LDH was determined to be approximately 4 nm (Fig. 1d), further confirming its ultrathin nature. The Fe proportion in the $NiZnFe_{12.9}$ LDH sample was determined to be 12.9% and 12.3%, as determined by ICP and EDS results (Fig. S5, ESI†). Elemental mapping of the NiZnFe LDH confirmed the uniform distribution of Ni, Zn, Fe, and O, providing evidence for the successful formation of the NiZnFe LDH composite (Fig. 1e).

The crystal structure of the different samples was analyzed using X-ray powder diffraction (XRD) measurements. The XRD patterns of NiZn LDH and $NiZnFe_x$ LDH exhibited the characteristic peaks of layered double hydroxides (Fig. 2a).[26] The peaks at 11.3° can be indexed as the (003) facet of typical Ni based LDH (PDF #38-0715). In comparison, when the Fe content was increased from 2.6 wt% to 23.7 wt%, the peak at 21.5° gradually increased, indicating the formation of $Fe(OH)_3$ phase. Besides, from the enlarged XRD patterns, we noticed a negative shift of the LDH (003) facet for all the Fe-containing catalysts compared to NiZn LDH. The results indicated that the Fe doping may cause the expansion of the NiZn LDH interlayer. The XRD results confirmed that the Fe species were both doped in the LDH lattice and formed in the $Fe(OH)_3$ phase, which is aligned with the HRTEM analysis. The FT-IR spectra of NiZn LDH and NiZnFe LDH are displayed in Fig. 2b. The absorption band located at 3435 cm^{-1} corresponds to the stretching vibrations of interlayer H_2O molecules and hydroxyl groups (–OH) on the surface. The band at around 1000 cm^{-1} is attributed to the vibration signal of –OH coordinated with the metal cations (Ni^{2+}, Zn^{2+}, Fe^{3+}) within the layers. Additionally, the peaks observed in the range of 400 to 800 cm^{-1} are attributed to the characteristic vibrations of metal–oxygen (M–O) and oxygen-bridged metal–oxygen–metal (O–M–O) bonds, where M represents Ni, Zn, and Fe, confirming the successful formation of the LDH structure.[27] To further investigate the elemental composition, the XPS spectra of both the NiZn LDH and $NiZnFe_{12.9}$ LDH composites were measured, revealing the presence of Ni, Zn, Fe, and O elements (Fig. S6, ESI†). These findings were consistent with the EDX analysis

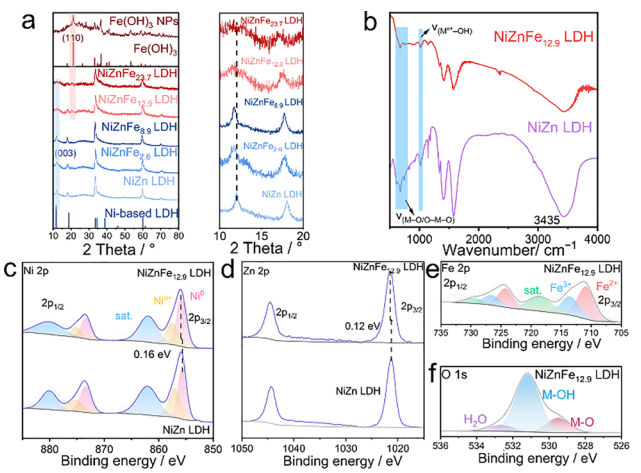

Fig. 2 (a) XRD patterns and (b) FT-IR spectrum of NiZn LDH and $NiZnFe_{12.9}$ LDH. The high-resolution Ni 2p (c), Zn 2p (d), Fe 2p (e) and O 1s (f) spectrum of different samples.

results, confirming the successful incorporation of Fe into the NiZn LDH structure.

The high-resolution XPS spectra of Ni 2p, Zn 2p, Fe 2p, and O 1s are displayed in Fig. 2c–f, providing detailed insights into the electronic states and chemical environments within the catalysts. The Ni 2p spectrum (Fig. 2c) is deconvoluted into four distinct peaks corresponding to Ni $2p_{3/2}$, Ni $2p_{1/2}$, and two satellite peaks. The primary binding energy for Ni $2p_{3/2}$ is located at 856.1 eV, indicating the dominance of Ni^{2+} in both NiZn LDH and $NiZnFe_{12.9}$ LDH.[20] In the Zn 2p spectrum (Fig. 2d), two peaks are observed at 1021.2 eV and 1044.1 eV, attributed to Zn $2p_{3/2}$ and Zn $2p_{1/2}$, respectively. A slight shift of 0.16 eV and 0.12 eV toward higher binding energies for the Ni $2p_{3/2}$ and Zn $2p_{3/2}$ peaks in $NiZnFe_{12.9}$ LDH, compared to NiZn LDH, suggests strong electronic interactions among Ni, Zn, and Fe within the LDH structure. These interactions are facilitated by the ligand (2-methylimidazole), highlighting partial substitution of Ni and Zn by Fe atoms. The Fe 2p spectrum (Fig. 2e) further confirms the incorporation of Fe, showing peaks at 710.6 eV (Fe^{2+} $2p_{3/2}$), 713.5 eV (Fe^{3+} $2p_{3/2}$), 723.8 eV (Fe^{2+} $2p_{1/2}$), and 726.6 eV (Fe^{3+} $2p_{1/2}$). This substantiates the successful introduction of Fe ions into the $NiZnFe_{12.9}$ LDH. Additionally, the O 1s spectrum (Fig. 2f) can be deconvoluted into three peaks: 529.7 eV (lattice oxygen from M–O bonding), 531.5 eV (oxygen species in M–OH), and 532.5 eV (adsorbed oxygen), collectively confirming the formation of the LDH structure.[28]

To further evaluate the hydrophilicity of the catalysts, contact angle tests were applied (Fig. S7, ESI†). The contact angles measured for clean Ni foam, NiZn LDH on Ni foam, and $NiZnFe_{12.9}$ LDH on Ni foam were 33.8°, 15.0°, and 6.9°, respectively. The significantly reduced contact angle for $NiZnFe_{12.9}$ LDH indicates a highly hydrophilic surface, which is a critical factor in enhancing water-splitting efficiency by facilitating water adsorption and reaction kinetics.

Based on the previous discussion, $NiZnFe_{12.9}$ LDH exhibits compositional and structural advantages, which are expected to contribute to improved electrochemical performance. The OER catalytic performance of different catalysts was acquired in a three-electrode setup with 1.0 M KOH as the electrolyte. Fig. 3a and b represent the linear sweep voltammetry (LSV) polarization curves for the OER at 5 mV s^{-1} with 95% iR-compensation and the comparison of the overpotential in 1 M KOH under an O_2 atmosphere. Using $NiZnFe_{2.6}$ LDH, $NiZnFe_{8.9}$ LDH, $NiZnFe_{12.9}$ LDH, $NiZnFe_{23.7}$ LDH and NiZn LDH as OER catalysts, all the Fe-containing catalysts display more effective OER performance than NiZn LDH. To be specific, the corresponding overpotential of $NiZnFe_{12.9}$ LDH at 10, 100 and 200 mA cm^{-2} is 191/232/246 mV, superior to $NiZnFe_{23.7}$ LDH (205/264/280 mV), $NiZnFe_{8.9}$ LDH (265/303/316 mV) and $NiZnFe_{2.6}$ LDH (313/401/453 mV) (Fig. 3b). The $NiZnFe_{12.9}$ LDH catalyst also demonstrates the lowest Tafel slope among all samples (35.6 mV dec^{-1}), which indicates the fastest reaction kinetics (Fig. 3c). Furthermore, the overpotential and Tafel slope of $NiZnFe_{12.9}$ LDH are even lower than those of previously reported Fe-containing materials in 1 M KOH (Table S1, ESI†).

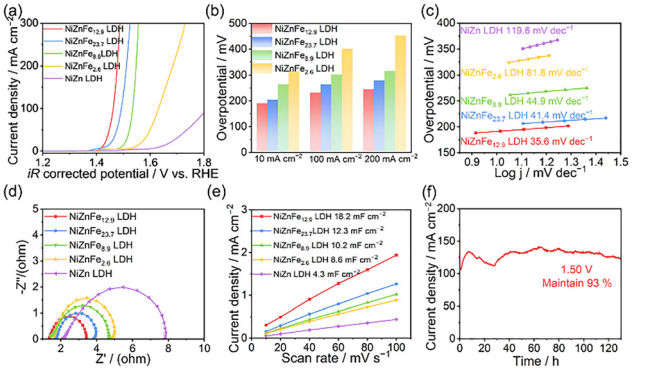

Fig. 3 (a) LSV curves of NiZn LDH and $NiZnFe_x$ LDH with different Fe contents. (b) Overpotential comparison at different current densities. (c) Corresponding Tafel plots, (d) EIS curves and (e) C_{dl} comparisons of the NiZn and $NiZnFe_x$ LDH catalysts. (f) Chronoamperometry measurements of $NiZnFe_{12.9}$ LDH.

To further examine the charge transfer properties of different catalysts, electrochemical impedance spectroscopy (EIS) was performed. The Nyquist plots for the various samples are presented in Fig. 3d. The electrocatalytic activity and conductivity were also reflected by the solution resistance (R_s) and charge transfer resistance (R_{ct}), which are summarized in Table S2 (ESI†). The lowest R_s and R_{ct} values of $NiZnFe_{12.9}$ LDH among the tested samples indicated a highest conductivity and a fastest electron transfer ability, and then boosted its OER kinetics as a result, which was consistent with the Tafel analysis. The number of active sites is a critical factor influencing the catalytic performance of the electrocatalysts. To evaluate the electrochemical properties of the $NiZnFe_{12.9}$ LDH catalyst, CV curves in the non-faradaic region (Fig. S8, ESI†) were recorded to determine the double-layer capacitance (C_{dl}). According to Fig. 3e, the C_{dl} value of $NiZnFe_{12.9}$ LDH was measured to be 18.2 mF cm^{-2}, which is significantly higher than that of other comparable catalysts. This increased capacitance further confirms the presence of a high density of active sites within the $NiZnFe_{12.9}$ LDH material. These findings validate that the moderate incorporation of Fe into the NiZn LDH structure effectively enhances its OER activity by increasing the number of active sites.

In order to investigate the interaction between the NiZn nanosheet support and the $Fe(OH)_3$ nanoparticles, we synthesized pure $Fe(OH)_3$ nanoparticles on Ni foam using a similar method, but without adding the Ni and Zn precursors. The corresponding SEM and TEM images are displayed in Fig. S9 (ESI†), which showed a severe aggregation. The LSV curves of $Fe(OH)_3$ nanoparticles and $NiZnFe_{12.9}$ LDH are shown in Fig. S10 (ESI†). The overpotential of $Fe(OH)_3$ nanoparticles at 10 mA cm^{-2} is 296 mV, much higher than the $NiZnFe_{12.9}$ LDH catalyst. Besides, we prepared $Fe(OH)_3$ nanoparticles and NiZn LDH separately. Followed by a physical mixing process of these samples through ultrasonication and grinding, and the Fe content was determined to be 13.8 wt%. Its STEM images and electrochemical performances are shown in Fig. S11 (ESI†). The $Fe(OH)_3$ particles show obvious aggregation and separation

from the NiZn LDH nanosheets. The overpotential of $Fe(OH)_3$ on the NiZn LDH catalyst at 10 and 100 mA cm^{-2} was tested to be 262 mV and 296 mV, and the Tafel slope was 66.39 mV dec^{-1}, inferior to the $NiZnFe_{12.6}$ LDH. These results further confirmed the interaction between $Fe(OH)_3$ and NiZn LDH in our one-pot synthesized samples.

The long-term stability of $NiZnFe_{12.9}$ LDH was evaluated *via* chronoamperometric measurements (Fig. 3f). The current density remained above 93% of its initial value over 125 hours at 120 mA cm^{-2} and 1.50 V, demonstrating excellent stability. A stability test was also performed for NiZn LDH for comparison (Fig. S12, ESI†), and the current density only displayed 50% retention after 6 hours. These results further highlight that the incorporation of Fe plays a crucial role in enhancing the catalytic stability of $NiZnFe_{12.9}$ LDH. To evaluate this, SEM and TEM images of the catalyst after the long-term stability test were analyzed (Fig. S13, ESI†). The images reveal that the nanosheet structure of $NiZnFe_{12.9}$ LDH remained largely unchanged, even after extended exposure to oxidation conditions. The $Fe(OH)_3$ nanoparticles retained a consistent size distribution with a mean size of 2.51 ± 0.62 nm, further indicating the stability of the material. Moreover, the Fe content was found to be approximately 10% after the stability test (Fig. S14, ESI†), suggesting that the $Fe(OH)_3$ nanoparticles exhibited negligible leaching during the reaction, thus confirming the robustness of the catalysts.

In conclusion, a highly dispersed $Fe(OH)_3$-decorated ultrathin NiZn LDH catalyst was successfully synthesized *via* a straightforward co-precipitation method. The unique ultrathin nanosheet structure maximizes the exposure of high-activity sites, significantly enhancing catalytic efficiency. The incorporation of $Fe(OH)_3$ nanoparticles introduces additional active sites and promotes efficient electron transfer, leading to optimized reaction kinetics and improved charge transfer dynamics. The optimized $NiZnFe_{12.9}$ LDH catalyst demonstrated exceptional OER performance, achieving a low overpotential of 191 mV at 10 mA cm^{-2} and exhibiting outstanding durability, maintaining consistent catalytic activity for over 120 hours at a current density of 120 mA cm^{-2} under alkaline conditions. These results underscore the effectiveness of this synthetic approach in creating high-performance LDH-based electrocatalysts and highlight its potential for advancing energy-related technologies.

The financial support for this work was provided by the National Key Research and Development Project of China (2022YFE0113800), National Natural Science Foundation of China (22102013), Natural Science Foundation of Chongqing (CSTB2024NSCQ-MSX0413) and Baseline Funds (BAS/1/1372-01-01) & Research Translation Funds (REI/1/4220-01-01) from King Abdullah University of Science and Technology (KAUST).

Data availability

The data supporting this article have been included as part of the ESI.†

Conflicts of interest

There are no conflicts to declare.

References

1 N. T. Suen, S. Fu., H. Q. Quan, N. Zhang, Y. J. Xu and H. M. Chen, *Chem. Soc. Rev.*, 2017, **46**, 337–3365.
2 Y. M. Shi, M. Y. Li, Y. F. Yu and B. Zhang, *Energy Environ. Sci.*, 2020, **13**, 4564–4582.
3 J. C. Li, C. Zhang, T. Zhang, Z. H. Shen, Q. W. Zhou, J. Pu, H. J. Ma, T. H. Wang, H. G. Zhang, H. M. Fan, Y. Y. Wang and H. X. Ma, *Chem. Eng. J.*, 2020, **397**, 11.
4 Z. Wang, J. Xu, J. H. Yang, Y. H. Xue and L. M. Dai, *Chem. Eng. J.*, 2022, **427**, 131498.
5 J. Y. Tian, F. L. Jiang, D. Q. Yuan, L. J. Zhang, Q. H. Chen and M. C. Hong, *Angew. Chem., Int. Ed.*, 2020, **59**, 13101–13108.
6 W. X. Ning, R. Wang, X. X. Li, M. H. Wang, H. G. Xu, H. Y. Lin, X. P. Fu, M. M. Wang, P. F. Liu and H. G. Yang, *Chem. Commun.*, 2023, **59**, 11803–11806.
7 M. Berger, A. Markus, S. Palkovits and R. Palkovits, *ChemElectroChem*, 2024, **11**, e202400457.
8 A. S. Darsan, P. Devi, P. Murugan and A. Pandikumar, *ACS Appl. Mater. Interfaces*, 2024, **16**(39), 52515–52528.
9 Y. Wei, F. C. Li and L. Liu, *RSC Adv.*, 2014, **4**, 18044–18051.
10 S. Wang, S. Qin, G. L. Yang, Y. C. Liu, T. R. Yang, Z. Y. Wang, X. H. Li, D. Liu and W. W. Lei, *ACS Appl. Mater. Interfaces*, 2024, **16**, 69725–69732.
11 P. Zhou, Y. Y. Wang, C. Xie, C. Chen, H. W. Liu, R. Chen, J. Huo and S. Y. Wang, *Chem. Commun.*, 2017, **53**, 11778–11781.
12 Y. X. Zhao, L. R. Zheng, R. Shi, S. Zhang, X. A. Bian, F. Wu, X. Z. Cao, G. I. N. Waterhouse and T. R. Zhang, *Adv. Energy Mater.*, 2020, **10**, 2002199.
13 D. P. Liu, Y. Du, T. Z. Li, H. H. Zhang, D. D. Liu, W. N. Zhang, H. Tang, Y. H. Hou, J. S. Li, S. C. Yan, T. Yu and Z. G. Zou, *Chem. Commun.*, 2020, **56**, 11465.
14 T. T. Sun, Z. F. Zhao, Z. K. Xu and S. Y. Lin, *Rare Met.*, 2023, **42**, 1453–1459.
15 D. J. Zhou, Z. Cai, Y. Jia, X. Y. Xiong, Q. X. Xie, S. Y. Wang, Y. Zhang, W. Liu, H. H. Duan and X. M. Sun, *Nanoscale Horiz.*, 2018, **3**, 532–537.
16 X. B. Hu, L. D. Zhang, S. Y. Li, J. Y. Chen, B. Y. Zhang, Z. Y. Zheng, H. Y. He, S. P. Luo and A. J. Xie, *New J. Chem.*, 2022, **46**, 19491–19500.
17 C. Feng, M. B. Faheem, J. Fu, Y. Q. Xiao, C. L. Li and Y. B. Li, *ACS Catal.*, 2020, **10**(7), 4019–4047.
18 J. D. Chen, F. Zheng, S. J. Zhang, A. Fisher, Y. Zhou, Z. Y. Wang, Y. Y. Li, B. B. Xu, J. T. Li and S. G. Sun, *ACS Catal.*, 2018, **8**(12), 11342–11351.
19 P. M. Bodhankar, P. B. Sarawade, G. Singh, A. Vinu and D. S. Dhawale, *J. Mater. Chem. A*, 2021, **9**, 3180–3208.
20 Q. Y. He, L. Han and K. Tao, *Chem. Commun.*, 2024, **60**, 1116.
21 W. Q. Li, H. Zhang, K. Zhang, Z. Z. Cheng, H. P. Chen, G. Tan, X. Feng, L. Y. Wang and S. C. Mu, *Chem. Commun.*, 2023, **59**, 4750.
22 B. R. Guo, H. H. Huo, Q. X. Zhuang, X. Q. Ren, X. X. Wen, B. L. Yang, X. X. Huang, Q. W. Chang and S. W. Li, *Adv. Funct. Mater.*, 2023, **33**, 2300557.
23 L. Trotochaud, S. L. Young, J. K. Ranney and S. W. Boettcher, *J. Am. Chem. Soc.*, 2014, **136**, 6744–6753.
24 W. Zhang, Y. Wang, H. Zheng, R. Li, Y. Tang, B. Li, C. Zhu, L. You, M. R. Gao, Z. Liu, S. H. Yu and K. Zhou, *ACS Nano*, 2020, **14**, 1971.
25 J. Zhao, Y. Guo, Z. Q. Zhang, X. L. Zhang, Q. Q. Ji, H. Zhang, Z. Q. Song, D. Q. Liu, J. R. Zeng, C. H. Chuang, E. H. Zhang, Y. H. Wang, G. Z. Hu, M. A. Mushtaq, W. Raza, X. K. Cai and F. Ciucci, *Nat. Nanotechnol.*, 2025, **20**, 57–66.
26 Z. W. Cai, J. Liang, Z. X. Li, T. Y. Yan, C. X. Yang, S. J. Sun, M. Yue, X. W. Liu, T. Xie, Y. Wang, T. S. Li, Y. S. Luo, D. D. Zheng, Q. Liu, J. X. Zhao, X. P. Sun and B. Tang, *Nat. Commun.*, 2024, **15**, 6624.
27 Z. L. Hsieh, M. C. Lin and J. Y. Uan, *J. Mater. Chem. A*, 2011, **21**, 1880.
28 J. D. Chen, F. Zheng, S. J. Zhang, A. Fisher, Y. Zhou, Z. Y. Wang, Y. Y. Li, B. B. Xu, J. T. Li and S. G. Sun, *ACS Catal.*, 2018, **8**, 11342–11351.

